Journal of Applied Polymer Science

Gas Permeation and Separation Properties of Polyimide/ZSM-5 Zeolite Composite Membranes Containing Liquid Sulfolane

Shinji Kanehashi, Hua Gu, Ryohei Shindo, Shuichi Sato, Tetsuo Miyakoshi, Kazukiyo Nagai
Department of Applied Chemistry, Meiji University, 1-1-1 Higashi-mita, Tama-ku, Kawasaki 214-8571, Japan
Correspondence to: K. Nagai (E-mail: nagai@meiji.ac.jp)

ABSTRACT: The preparation, characterization, and gas permeation properties of novel composite membranes containing polyimide (PI), liquid sulfolane (SF), and zeolite (ZSM-5) were investigated to address the interface defects between the PI and the zeolite. The free-standing composite membranes were prepared by the solvent casting method. The gas permeability of the PI+ZSM-5 membrane was higher than that of PI, whereas its gas selectivity was significantly reduced, suggesting that these results are attributed to the interface defects. The CO_2 selectivity of PI+ZSM-5+SF was higher than those of the PI+ZSM-5 membranes because of the introduction of liquid SF into the interface defects. Furthermore, liquid SF enhanced the CO_2/H_2 selectivity near the recent upper bound. Therefore, the use of liquid SF could be an effective approach to preventing interface defects and increasing the CO_2 selectivity, particularly for CO_2/H_2. © 2012 Wiley Periodicals, Inc. J. Appl. Polym. Sci. 128: 3814–3823, 2013

KEYWORDS: composites; polyimides; membranes

Received 21 June 2012; accepted 4 September 2012; published online 12 October 2012
DOI: 10.1002/app.38572

INTRODUCTION

Polymer membrane-based gas separation is an example of effective separation technologies that are low cost and low energy.[1] CO_2 gas separation has attracted significant interest because of the recent serious environmental problems arising from global warming. For example, there are CO_2/H_2 separation for hydrogen purification in precombustion processes (integrated gasification combined cycle), CO_2/N_2 separation, which involves CO_2 capture from power plants and iron foundries for the carbon dioxide capture and storage (CCS) process for postcombustion processes, CO_2/CH_4 separation for natural gas purification and CO_2 concentration from biogas, and CO_2/O_2 separation for food packaging applications.[2–4] In these applications, high gas permeability, selectivity, mechanical strength, and processability of polymer membrane materials are desirable characteristics.

Fluorine-containing polyimides (PIs) show high mechanical strength, chemical resistance, and thermal stability. Furthermore, these materials exhibit effective CO_2 separation performance and high processability because of their solvent solubility compared with other conventional PIs. This high solubility is attributed to the presence of fluorine.[5] In particular, a fluorine-containing PI composed of 4,4-hexafluoroisopropylidene diphtalic anhydride (6FDA) and 2,3,5,6-tetramethyl-1,4-dienylene diamine (TeMPD) shows high gas permeability based on the high free volume.[6]

In the past decades, several approaches to enhancing gas separation performance have been investigated, including the use of composites prepared from polymer and inorganic fillers such as zeolites,[7–11] silica,[12–14] carbon molecular sieves,[15,16] and carbon nano tube.[17] A number of reviews on the performance of mixed-matrix membranes (MMMs) have also been published.[18,19]

Polyimide-zeolite MMMs have recently attracted research interest. In MMMs, a continuous, well-dispersed inorganic filler in the polymer membranes is desired. However, the gas separation performance of MMMs is significantly reduced because of the interface defects between the polymer and the inorganic filler.[20–24] These interface defects are attributed to the weak interaction between the polymer and the filler. Thus, a number of approaches have been applied to improve these membrane interface defects. Examples are the surface modification of zeolite fillers via a silane coupling reaction[7,18,19,25] and the addition of a compatibilizing agent into the membranes.[26]

In this study, we focus on the improvement of the interface defects between the polymer and the zeolite by introducing liquid sulfolane (SF), which has high CO_2 affinity, which indicates high CO_2 selectivity. SF, a polar solvent with a high boiling point, is used to separate sour gas components and extract aromatic components from petroleum.[27] Several studies on the use of CO_2 separation membranes containing SFs have been reported in Refs. 28 and 29. In this study, we prepared

zeolite-polyimide composite membranes containing liquid SFs to prevent the formation of interface defects between the polymer and the zeolite. The physical and thermal properties as well as the gas separation performance were investigated in terms of the SF content.

EXPERIMENTAL

Chemicals

The 6FDA-TeMPD PI monomers, namely, 6FDA and TeMPD, were purchased from Tokyo Chemical Industry (Japan) and Aldrich (USA), respectively. These monomers were dried in vacuum prior to use. The ZSM-5 zeolite was purchased from Zeolyst International and then dried in vacuum prior to use. The properties of the ZSM-5 zeolite are as follows: Si/Al = 30, real density = 1.768 g/cm^3, and pore diameter = 0.54 nm to 0.55 nm.[30,31] The particle size, as determined via scanning electron microscopy (SEM), ranges from 0.3 to 3.0 μm. SF was purchased from Tokyo Chemical Industry (Japan) and used without further purification.

Membrane Preparation

6FDA-TeMPD PI was synthesized according to our previous study.[6] Isotropic dense PI membranes were prepared by casting a filtered 5.0 wt % solution of the polymer in dichloromethane onto glass dishes. The ZSM-5 zeolite was dried for 72 h under vacuum and then added into the SF solution, at a zeolite content of 15 wt % of the polymer weight. The SF content varied from 0 to 33 wt % because liquid SF bleeds out of the membrane when the content exceeds 33 wt %. The SF-adsorbed ZSM-5 zeolite was added to the 5% filtered PI solution. Subsequently, the solution was cast onto a flat-bottomed glass dish, and the solvent was allowed to evaporate slowly over a period of $\sim$ 72 h. The well-dried membrane was used considering the effect of the membrane thickness, which varied from 40 to 60 μm with a measurement uncertainty of $\pm$2 μm. Therefore, four kinds of membranes, 6FDA-TeMPD (PI), 6FDA-TeMPD-ZSM-5 zeolite (PI+ZSM-5), 6FDA-TeMPD-ZSM-5 zeolite containing SF (PI+ZSM-5+SF), and 6FDA-TeMPD containing SF (PI+SF) were prepared.

Membrane Characterization

All characterization data were obtained in the membrane state using a minimum of three samples to confirm the reproducibility of the experimental results.

The characterization of PI membranes were conducted via proton and carbon nuclear magnetic resonance (^{1}H and ^{13}C NMR) spectroscopies using a JNM-ECA500 spectrometer (JEOL, Tokyo, Japan). The measurements were performed in chloroform solutions. The SF content in the PI membrane was determined via ^{1}H-NMR analysis.

Fourier transform infrared (FTIR) spectroscopy was performed on a FT/IR-4100 (JASCO, Tokyo, Japan) spectrometer equipped with an attenuated total reflectance (ATR) accessory at 23 $\pm$ 1°C. Each spectrum was averaged over 64 scans at a resolution of 2 cm^{-1}.

The depth of penetration (Dp) of the IR beam can be calculated from eq. (1):[32]

$$Dp = \frac{\lambda}{2\pi n_1 \sqrt{\sin^2\theta - \left(\frac{n_2}{n_1}\right)^2}} \quad (1)$$

where λ is the wavelength of the incident beam at atmospheric conditions, θ is the incident angle, and n_1 and n_2 are the refractive indices of the ATR–IR crystal ($n_1 = 2.4$) and the PI sample ($n_2 = 1.534$), respectively.[33]

SEM was performed using a high-resolution field emission scanning electron microscope (S5200, JEOL, Tokyo, Japan).

Orthoscopic observation was conducted using an Olympus BH-2 polarization microscope (POM, Olympus, Tokyo, Japan) under a cross-Nicol condition. Polarization images were observed at 530 nm under an additive color using a sensitive color plate.

The membrane density (ρ) was measured through the volumetric method at 23 $\pm$ 1°C using the given membrane weight and volume.

Wide-angle X-ray diffraction (WAXD) measurement was performed on a Rint 1200 X-ray diffractometer (Rigaku, Tokyo, Japan) at a scanning speed of 2°/min using a Cu Kα radiation source at 40 kV and 20 mA at a dispersion angle from 0° to 50°. The *d*-spacing, which represents the mean distance between polymer chains, was calculated from Bragg's conditions.[34]

Thermogravimetric analysis (TGA) was performed on a Pyris 1 TGA thermogravimetric analyzer (PerkinElmer, Shelton, CT). The polymer sample (ca. 1.0 mg) was heated in a platinum pan from 50 to 800°C at a heating rate of 10°C/min under a nitrogen atmosphere at a flow rate of 60 mL/min. The SF content was calculated from the decrease ratio at the SF decomposition temperature. Differential scanning calorimetry (DSC) was used to analyze the PI and PI+ZSM-5 membranes using a Diamond DSC (PerkinElmer, Shelton). The sample pan-kit alum was made of aluminum. The heat scan was conducted from 350 to 500°C at a heating rate of 10°C/min under a nitrogen atmosphere. The glass transition temperature (T_g) was determined as the middle point of the endothermic transition.

Gas Permeation

The H_2, O_2, N_2, CO_2, and CH_4 pure gas permeabilities were determined via constant-volume/variable-pressure method, which measures the steady-state gas flux through a membrane of known thickness under a given pressure difference. All permeation data were determined at 35°C using a minimum of three samples to ensure the reproducibility of the experimental results. The upstream gas pressure ranged from 75 to 77 cmHg, whereas the downstream is under vacuum.

The gas permeation coefficient, P [cm^3 (STP) cm/(cm^2 s cm Hg)], was determined using the following equation:[34,35]

$$P = \frac{dp}{dt}\frac{273V}{760(273+T)}\frac{1}{A}\frac{1}{p}\ell \quad (2)$$

where dp/dt is the pressure increase in time, t, at the steady state; V (cm^3) is the downstream volume, T (°C) is the temperature,

Applied Polymer SCIENCE

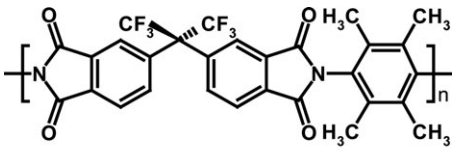

Figure 1. Chemical structures of the 4,4 -(hexafluoroisopropylidene) diphthalic anhydride (6FDA)-2,3,5,6-tetramethyl-1,4-phenylenediamine (TeMPD) polyimide and sulfolane.

A (cm^2) is the effective membrane area, p (cmHg) is the upstream pressure, and ℓ (cm) is the membrane thickness. The gas molecules were permeated through a membrane from the upper side and cast to the bottom side. The ideal gas selectivity, α, was calculated using the ratio of the permeability coefficient of Gas A over that of Gas B:

$$\alpha = \frac{P_A}{P_B} \tag{3}$$

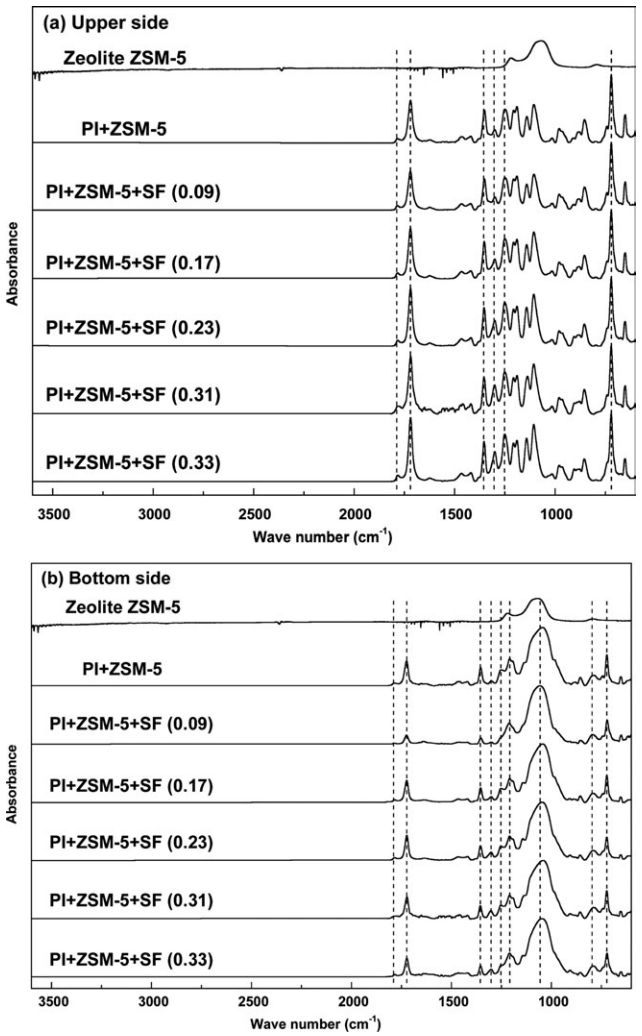

Figure 2. Attenuated total reflectance-Fourier transform infrared (ATR–FTIR) spectra of polyimide composite membranes: (a) upper side of the polyimide + zeolite (PI+ZSM-5) and PI+ZSM-5+sulfolane (SF) composites, and (b) bottom side of the PI+ZSM-5 and PI+ZSM-5+SF composite membranes.

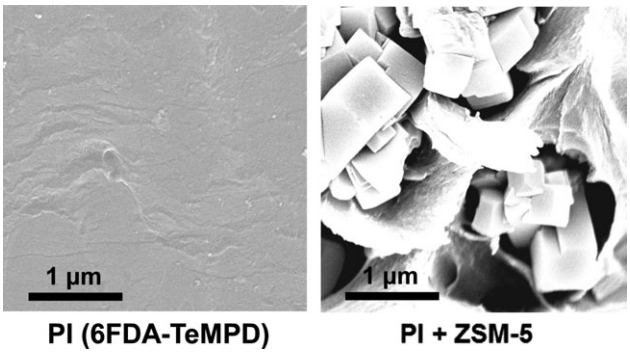

Figure 3. Scanning electron microscopy (SEM) images of the cross-section of the PI and PI+ZSM-5 composite membranes.

RESULTS AND DISCUSSION

Membrane Characterization

^{1}H-NMR, ^{13}C-NMR, and FTIR analyses were performed on the PI to confirm the chemical structures shown in Figure 1. The PI membranes showed effective membrane-forming ability regardless of the zeolite and SF contents. No chemical reaction occurred between the PI, the zeolite, and SF in the composite membranes, as confirmed by the similarity in the ^{1}H- and ^{13}C-NMR results. Therefore, these results indicate that the additive chemical bond between the PI, zeolite, and SF was not formed.

The ATR–IR peaks corresponding to the PIs (e.g., 1787 cm^{-1} (C=O asymmetric stretching), 1725 cm^{-1} (C=O symmetric stretching), 1354 cm^{-1} (C—N stretching), 1256 cm^{-1} (C—F stretching), and 724 cm^{-1} (C=O bending)) were observed on both sides of all the membranes. The SF absorption at 1299 cm^{-1} (O=S=O asymmetric vibration) in the PI+SF membrane increased with increasing SF content. This result suggests that the SF did not form domains in the membranes but was instead well dispersed. Therefore, these results illustrate the high compatibility of the PI and SF. Figure 2 shows the ATR–FTIR spectra of the top and bottom surfaces of the PI+ZSM-5, and PI+ZSM-5+SF. The zeolite specific peak at 1069 cm^{-1} (internal vibrations of Si and the ALO_4 tetrahedra) was observed only from the bottom sides of the PI+ZSM-5 and PI+ZSM-5+SF membranes. The SF peaks on both sides of the membranes increased with increasing SF content. ATR–FTIR results show the state at a depth of 1 to 2 μm from the membrane surface. Hence, the PI+ZSM-5 and PI+ZSM-5+SF membranes exhibit graded structures in the form of zeolites at the bottom sides of the membranes.

Figure 3 shows the SEM images of the cross-sectional PI and PI+ZSM-5 membranes. A homogeneous dense structure was observed in the 6FDA-TeMPD base PI membrane, whereas some voids $\sim$ 2 μm in size were formed between the PI and the zeolite in the PI+ZSM-5 membrane. This result suggests the

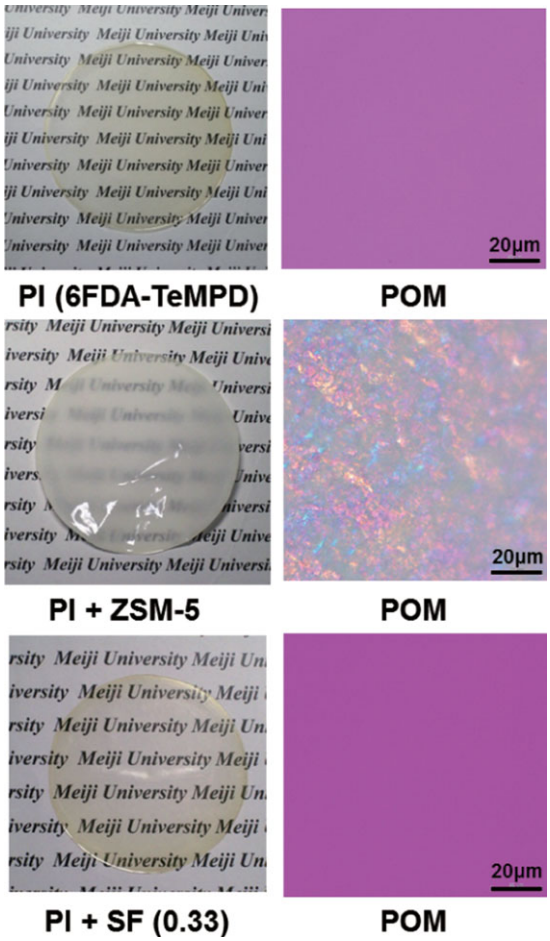

Figure 4. Photographs and the polarization microscopy (POM) images of PI, PI+ZSM-5 composites, and PI+SF (33 wt %) membranes. [Color figure can be viewed in the online issue, which is available at wileyonlinelibrary.com.]

presence of interface defects, which are attributed to the weak interaction between the polymer and the zeolite.[20]

On the basis of the SEM images, the ratio of the interface defect between the PI and the zeolite in the PI+ZSM-5 membrane was estimated at 15–20%. The SF density used in this study is 1.261 g/cm^3. Therefore, the SF amount required to fill the interface defects is ~ 12–16 wt %. The PI+ZSM-5+SF SF content in excess of 17 wt % was introduced into the space between the PI and the zeolite.

Photographs and POM images of the PI, PI+ZM-5, PI+SF (33 wt%), and PI+ZSM-5+SF membranes are shown in Figures 4 and 5. All membranes in this study exhibit the characteristics of a freestanding membrane. In Figure 4 the PI membrane displays a slight yellow transparent color, whereas PI+ZSM-5 exhibit a cloudy transparency because of the presence of the zeolite. The POM images also show no contrast between the PI and PI+SF membranes, indicating that these membranes exhibit amorphous structures. Color contrasts that reflect the crystalline structure of the zeolite was observed in the PI+ZSM-5 and PI+ZSM-5+SF membranes. The physical properties of these PI membranes are summarized in Table I. The SF contents of the PI+ZSM-5+SF and PI+SF membranes calculated from the ^{1}H-NMR results are in agreement with the feed. Therefore, the liquid SF did not evaporate from the membranes but instead remained in the PI matrices. The membrane densities of PI and PI+ZSM-5 are 1.324 and 1.361 g/cm^3, respectively, as determined via the volumetric method. The results indicate that the zeolite in the membrane increased the membrane density. Regardless of the SF content, the PI+ZSM-5+SF membrane density is ~ 1.35 g/cm^3, which is lower than that of PI+ZSM-5. These results show that the zeolite domain in the PI+ZSM-5+SF membrane was stable and was not affected by the SF content. By contrast, the membrane density of the PI+SF membrane decreased from 1.324 to 1.230 g/cm^3 as the SF content increased, thus suggesting that the SF in the membrane was well-dispersed in the PI matrices.

The WAXD patterns of the PI composite membranes are shown in Figure 6. The single broad halo observed in the PI and PI+SF membranes indicates that these PIs display amorphous structures. The sharp peaks at around 7° to 8° and 23° to 25° are observed on both sides of the PI+ZSM-5 and PI+ZSM-5+SF membranes. As expected, the ATR-IR peak intensity of the bottom side is stronger than that of the upper side. Therefore, the PI+ZSM-5 and PI+ZSM-5+SF membranes at the bottom side of the membranes exhibit graded structures in the form of zeolites. Except for the sharp peaks that correspond to the zeolite, the WAXD profiles of all membranes show a single broad halo, suggesting that the PIs are completely amorphous structure. The similar *d*-spacings of the PI and PI+ZSM-5 membranes (6.5 Å), as calculated from the Bragg condition, indicate that the PI *d*-spacing was not affected by the zeolite. Moreover, the *d*-spacing values of the PI+ZSM-5+SF and PI+SF membranes decreased from 6.5 to 5.4 Å with the increase in the SF content regardless of the presence of zeolite. These results confirm the introduction of the membrane SF into the PI matrices, which resulted in the decrease in the PI membrane free volume.

Figure 7 shows the TGA curves of the PI membranes. The PI and PI+ZSM-5 membranes displayed one-step thermal decomposition behaviors, as shown by the decomposition at 531 and 535°C, respectively. Therefore, the zeolite improved the thermal stability of the PI. On the other hand, two-step decompositions, which started at 100 and 530°C, were observed in the PI+ZSM-5+SF and PI+SF membranes. The boiling point of SF is 280°C. The first decomposition was based on the volatilization of SF, whereas the second is the decomposition of PI segments in the PI and PI+ZSM-5 membranes. The PI segments in PI and PI+SF membranes showed the same decomposition temperatures, thus confirming that the liquid SF in the membrane did not affect the PI rigidity. Table I shows that the decomposition temperature of the PI segments in the PI+ZSM-5+SF and PI+SF membranes are 535 and 530°C, respectively, regardless of the SF content. The residual weights of the PI+ZSM-5 and PI membranes at 800°C are ~ 62 and 51 wt %, respectively. On the basis of these results, the zeolite content was estimated at ~ 14.7 wt %, which is consistent with the 15 wt % feed. The T_g values of the PI and PI+ZSM-5 membranes are 424 and 444°C, respectively, as determined via DSC measurements, suggesting that the zeolite in the membrane considerably enhanced the PI thermal stability. DSC measurements for the PI+ZSM-5+SF

Applied Polymer SCIENCE

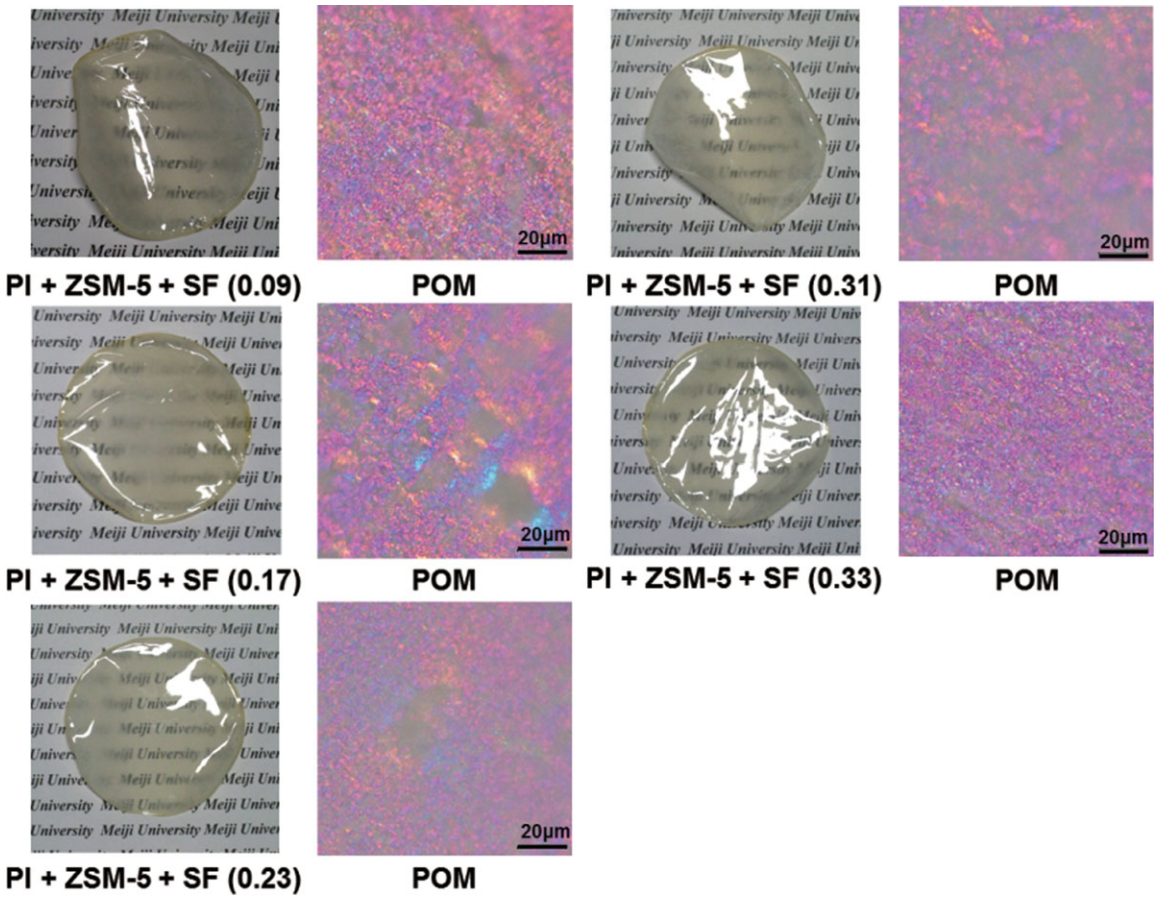

Figure 5. Photographs and POM images of PI+ZSM-5+SF composite membranes. [Color figure can be viewed in the online issue, which is available at wileyonlinelibrary.com.]

and PI+SF membranes were not performed because the SF component volatilizes at temperatures above 100°C, based on the TGA results for the PI+ZSM-5+SF and PI+SF membranes.

Gas Permeation and Separation

The gas permeation measurement results at 35°C for all PI membranes are summarized in Table II. Figure 8 shows the pure gas permeability coefficients at 35°C as a function of the

Table I. Physical and Thermal Properties of PI and PI-ZSM-5 Zeolite Composite Membranes Containing 0 to 33 wt % SF

	Sulfolane content				
Polymer	In feed	^{1}H-NMR	Membrane density (g/cm^3)	d-spacing (Å)[a]	T_d (°C)[b]
PI	0	0	1.323 ± 0.029	6.5 ± 0.1	531 ± 1
PI + ZSM-5	0	0	1.361 ± 0.010	6.5 ± 0.1	535 ± 1
PI + ZSM-5 + SF	0.09	0.09 ± 0.01	1.349 ± 0.003	6.0 ± 0.1	534 ± 1
	0.17	0.17 ± 0.01	1.348 ± 0.006	5.8 ± 0.1	534 ± 1
	0.23	0.23 ± 0.01	1.348 ± 0.005	5.7 ± 0.1	535 ± 2
	0.31	0.31 ± 0.01	1.335 ± 0.027	5.5 ± 0.1	535 ± 1
	0.33	0.33 ± 0.01	1.344 ± 0.002	5.4 ± 0.1	535 ± 2
PI + SF	0.09	0.09 ± 0.01	1.307 ± 0.009	6.0 ± 0.1	531 ± 5
	0.17	0.17 ± 0.01	1.292 ± 0.019	5.8 ± 0.1	528 ± 1
	0.23	0.23 ± 0.01	1.271 ± 0.020	5.7 ± 0.1	530 ± 1
	0.31	0.31 ± 0.01	1.234 ± 0.029	5.4 ± 0.1	530 ± 1
	0.33	0.33 ± 0.01	1.230 ± 0.012	5.4 ± 0.1	531 ± 1

[a]Values of polyimide, [b]Decomposition temperature of polyimide.

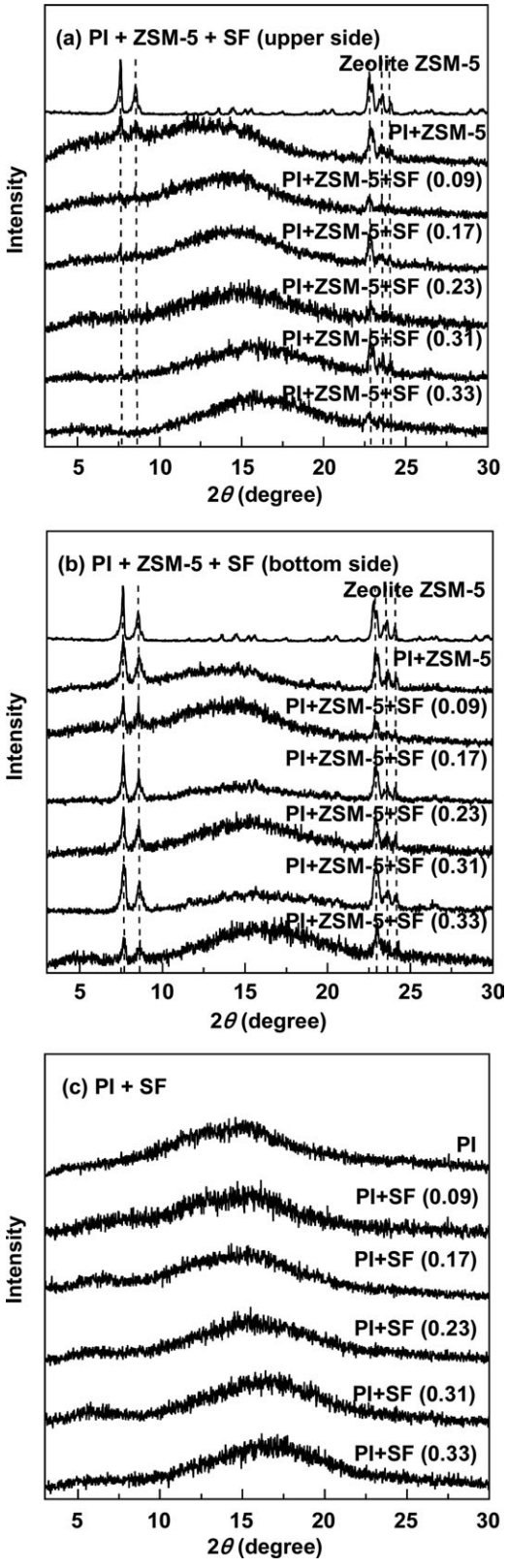

Figure 6. Wide-angle X-ray diffraction (WAXD) patterns of PI composite membranes: (a) upper side of PI+ZSM-5 and PI+ZSM-5+SF composites, (b) bottom side of PI+ZSM-5 and PI+ZSM-5+SF composites, and (c) PI and PI+SF membranes.

SF content in the PI+ZSM-5+SF and PI+SF membranes. The 0 wt % SF data in Figure 8 represent the gas permeabilities of PI+ZSM-5 and PI. The gas permeabilities of the PI+ZSM-5 membrane are higher than those of PI. For example, the methane permeability of PI+ZSM-5 is three times higher than that of PI. The increase in the gas permeability can be attributed to the interfacial defects between the PI and the zeolite in the PI+ZSM-5 membrane. On the other hand, the H_2 gas permeability of the PI+ZSM-5+SF and PI+SF membranes decreased with increasing SF content. Other gas permeability values also decreased. The decrease stopped when the SF content reached 17 wt %, and became nearly stable between 17 and 33 wt %. This decrease in the gas permeability can be attributed to the introduction of SF into the PI matrices. The results also confirm the high compatibility between the PI and SF.

The gas permeability coefficients of all PI membranes decreased in the following order:

$$\mathrm{PI}: CO_2 > H_2 > O_2 > N_2 > CH_4$$

$$\mathrm{PI{+}ZSM-5}: CO_2 > H_2 > O_2 > CH_4 > N_2$$

$$\mathrm{PI{+}ZSM{-}5{+}SF, PI{+}SF}: CO_2 > H_2 > O_2 > CH_4 > N_2$$

Except for PI, the order of the gas permeability coefficients was the same regardless of the SF content. In addition, the order in

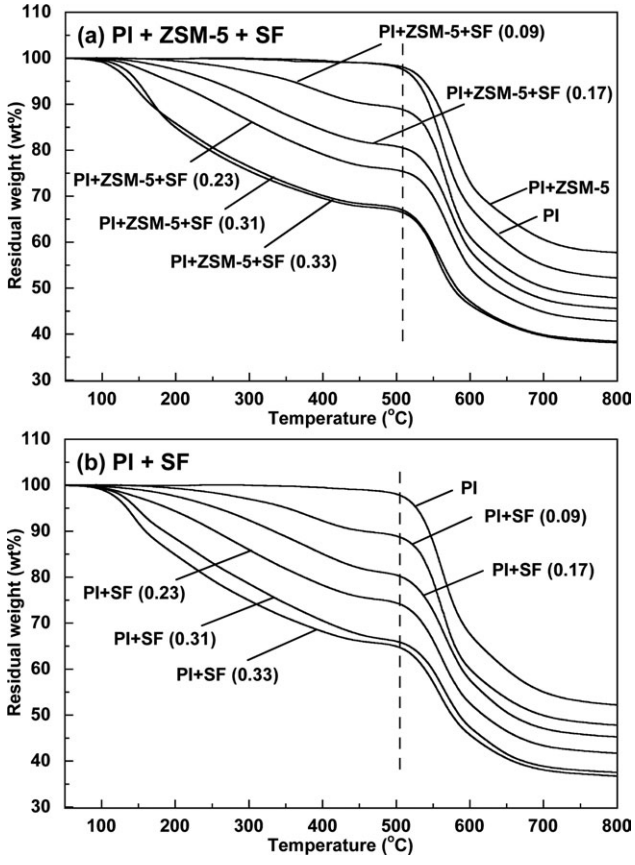

Figure 7. Thermogravimetric (TG) curves of PI membranes (a) PI+ZSM-5 and PI+ZSM-5 + SF composites and (b) PI and PI+SF membranes.

Table II. Gas Permeability Coefficients of PI and PI-ZSM-5 Zeolite Composite Membranes Containing 0 to 33 wt % SF

Polymer	Sulfolane content[a]	Permeability (cm^3 (STP) cm/(cm^2 s cm Hg) × 10^{-10})				
		H_2	O_2	N_2	CO_2	CH_4
PI	0	963 ± 46	247 ± 25	74.4 ± 8.0	1156 ± 96	62.1 ± 18
PI + ZSM-5	0	1268 ± 62.4	335 ± 25	164 ± 10	1492 ± 110	203 ± 20
PI + ZSM-5 + SF	0.09 ± 0.01	268 ± 13	52.7 ± 2.6	16.2 ± 0.8	293 ± 15	15.8 ± 0.8
	0.17 ± 0.01	99.3 ± 5.0	18.0 ± 0.8	5.6 ± 0.3	123 ± 6	6.5 ± 0.9
	0.23 ± 0.01	70.0 ± 4.8	16.4 ± 3.8	4.6 ± 0.2	104 ± 5	5.8 ± 0.8
	0.31 ± 0.01	48.2 ± 2.4	13.0 ± 0.7	3.7 ± 0.2	101 ± 5	5.6 ± 1.1
	0.33 ± 0.01	44.4 ± 3.9	11.6 ± 0.8	3.4 ± 0.2	88.4 ± 2.3	5.2 ± 1.0
PI + SF	0.09 ± 0.01	179 ± 20	34.0 ± 4.6	10.3 ± 1.2	173 ± 36	10.7 ± 2.5
	0.17 ± 0.01	72.1 ± 3.5	16.2 ± 1.4	4.6 ± 0.2	109 ± 5	6.0 ± 0.3
	0.23 ± 0.01	64.0 ± 3.2	13.6 ± 2.1	4.2 ± 0.2	102 ± 5	5.2 ± 0.4
	0.31 ± 0.01	43.2 ± 2.2	12.3 ± 0.6	3.5 ± 0.2	99.1 ± 5.0	5.0 ± 0.3
	0.33 ± 0.01	34.4 ± 1.6	10.0 ± 1.2	3.3 ± 0.1	84.6 ± 10.4	4.5 ± 0.3

[a]Determined by NMR analysis.

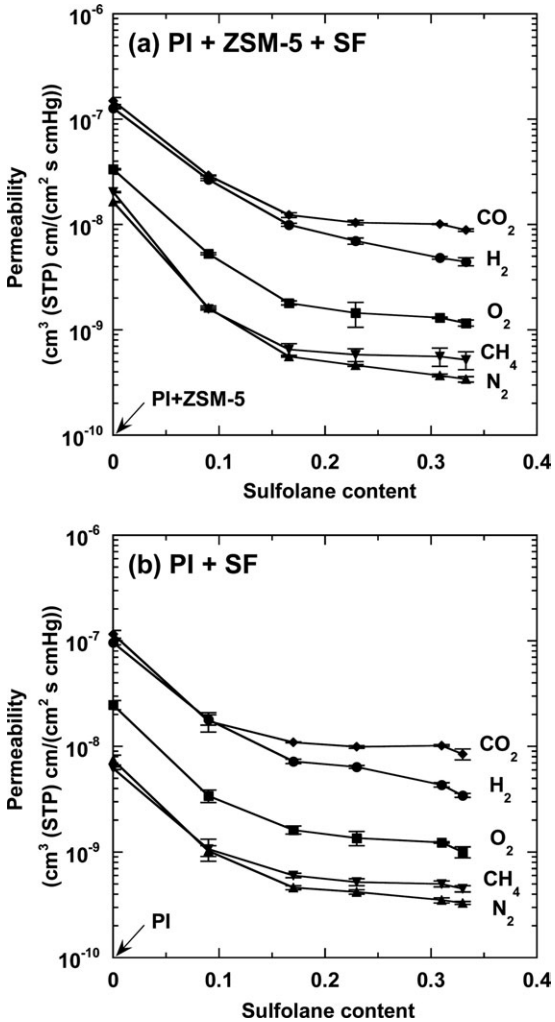

Figure 8. Pure gas permeability of PI membranes at 35°C as a function of the SF content (a) PI+ZSM-5 and PI+ZSM-5+SF composites and (b) PI and PI+SF membranes.

each membrane did not follow the trend of either the gas size or the gas condensability. Instead, the order depended on the balance between the diffusivity and solubility, which are strongly affected by the gas size and condensability.

To investigate the effect of zeolite on the gas permeability coefficients in the PI+ZSM-5+SF membrane, the permeability ratio was calculated using eq. (4):

$$Permeability\ ratio = \frac{P_{\mathrm{PI+ZSM\text{-}5+SF}}}{P_{PI+SF}} \tag{4}$$

where $P_{\mathrm{PI+ZSM\text{-}5+SF}}$ and $P_{\mathrm{PI+SF}}$ represent the gas permeability coefficients of the PI+ZSM-5+SF and PI+SF membranes, respectively. The relationship between the gas permeability ratio and the SF content is illustrated in Figure 9. The ratios of all the gas permeability coefficients in the PI+ZSM-5+SF membrane are all above 1. Thus, the gas permeabilities of PI+ZSM-5

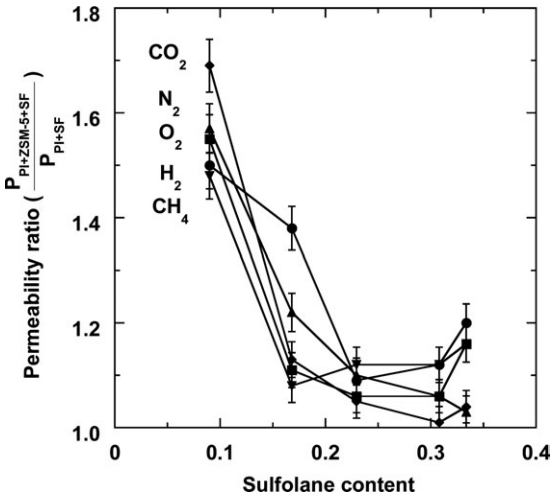

Figure 9. Increase in the gas permeability ratio of PI+ZSM-5+SF/PI+SF membranes at 35°C as a function of the SF content.

Table III. Gas Selectivity of PI and PI-ZSM-5 Zeolite Composite Membranes Containing 0 to 33 wt % SF

Polymer	Sulfolane content[a]	Gas selectivity			
		CO_2/N_2	CO_2/CH_4	CO_2/H_2	O_2/N_2
PI	0	15.5 ± 0.5	18.6 ± 0.3	1.3 ± 0.1	3.1 ± 0.1
PI + ZSM-5	0	9.1 ± 0.2	7.3 ± 0.1	1.3 ± 0.1	2.0 ± 0.1
PI + ZSM-5 + SF	0.09 ± 0.01	18.1 ± 0.5	18.6 ± 0.6	1.1 ± 0.1	3.2 ± 0.2
	0.17 ± 0.01	22.1 ± 0.7	18.9 ± 1.2	1.2 ± 0.1	3.2 ± 0.1
	0.23 ± 0.01	22.5 ± 1.6	17.9 ± 1.1	1.5 ± 0.2	3.6 ± 0.8
	0.31 ± 0.01	27.2 ± 0.5	18.0 ± 1.2	2.1 ± 0.1	3.5 ± 0.3
	0.33 ± 0.01	26.2 ± 0.8	17.1 ± 2.5	2.0 ± 0.1	3.5 ± 0.3
PI + SF	0.09 ± 0.01	16.6 ± 1.5	16.4 ± 0.6	1.0 ± 0.1	3.3 ± 0.2
	0.17 ± 0.01	23.3 ± 0.4	17.1 ± 0.9	1.5 ± 0.2	3.5 ± 0.1
	0.23 ± 0.01	23.9 ± 0.4	19.1 ± 1.5	1.5 ± 0.1	3.3 ± 0.7
	0.31 ± 0.01	28.7 ± 1.0	20.2 ± 0.5	2.4 ± 0.1	3.6 ± 0.2
	0.33 ± 0.01	25.6 ± 3.0	18.8 ± 2.1	2.5 ± 0.4	3.3 ± 0.6

[a]Determined by NMR analysis.

+ SF are all larger than those of the PI+SF membrane regardless of the SF content. Interestingly, the permeability ratio decreased until the SF content reached 17 wt %. For example, the permeability ratio of the PI+ZSM-5+SF membrane at the SF content of 9 wt % is 1.5–1.7 times higher than that of the PI+SF, whereas the ratio at 31 wt % SF is 1.0–1.2 times higher. As previously mentioned, a 12 to 16 wt % SF is required to fill the interface defects. The amount of SF in the PI+ZSM-5+SF and PI+SF membranes in excess of 17 wt % could be dispersed into the PI matrices, which can result in a decrease in the gas permeability. Therefore, the introduction of SF into the interface defects as well as into the PI matrices resulted in the higher permeability of PI+ZSM-5+SF (9 wt %) compared with that of the PI+SF membrane. When the SF content exceeded 17 wt %, the excess SF amount filled the PI matrices, which resulted in the decrease in the gas permeability.

The ideal gas selectivities of the PI+ZSM-5+SF and PI+SF membranes at 35°C are summarized in Table III. Figure 10 shows the gas selectivity at 35°C as a function of the SF content of the PI+ZSM-5+SF and PI+SF membranes. The 0 wt % SF data in Figure 10 represent the gas selectivities of PI+ZSM-5 and PI. As expected, the gas selectivities of the PI+ZSM-5 membrane are all lower than those of the PI membranes because of the interface defects between the PI and the zeolite. On the other hand, the selectivities of the PI+ZSM-5+SF membrane increased with increasing SF content. For example, the selectivity for CO_2/N_2 is three times higher than that of the PI membrane, whereas that for CO_2/H_2 is two times higher. By contrast, the selectivity for O_2/N_2 is nearly constant regardless of the SF content. Therefore, the increase in the CO_2 selectivity could indicate an increase in the CO_2 solubility attributable to the presence of SF, which has high affinity for CO_2. These results suggest that the SF did not affect the noncondensable gas pairs such as O_2/N_2 and increased the selectivity for CO_2/noncondensable pairs. In addition, the selectivities of PI+ZSM-5+SF are nearly similar to those of the PI+SF membranes at all

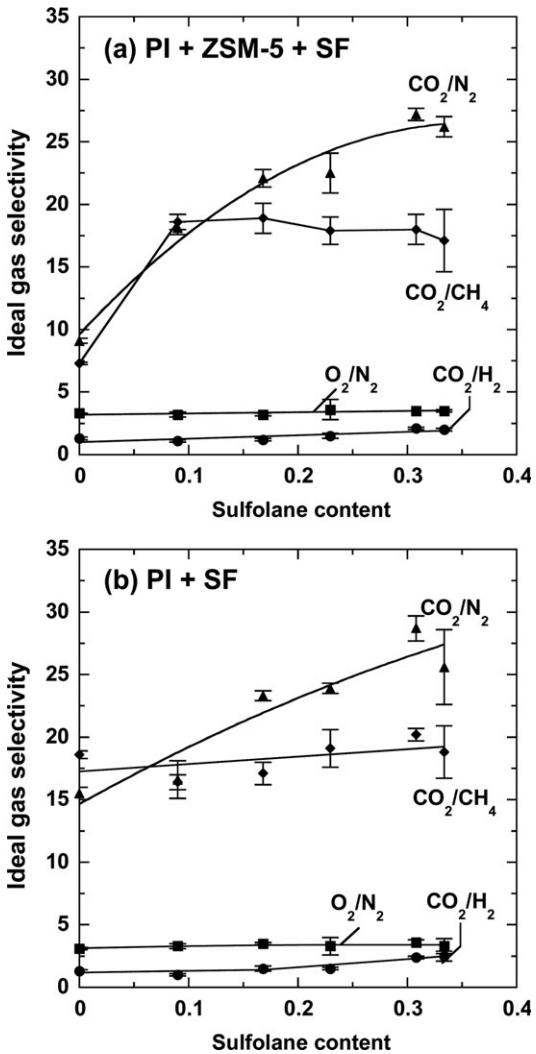

Figure 10. Pure gas selectivity in PI membranes at 35°C as a function of the SF content (a) PI+ZSM-5 and PI+ZSM-5+SF composites and (b) PI and PI + SF membranes.

Applied Polymer SCIENCE

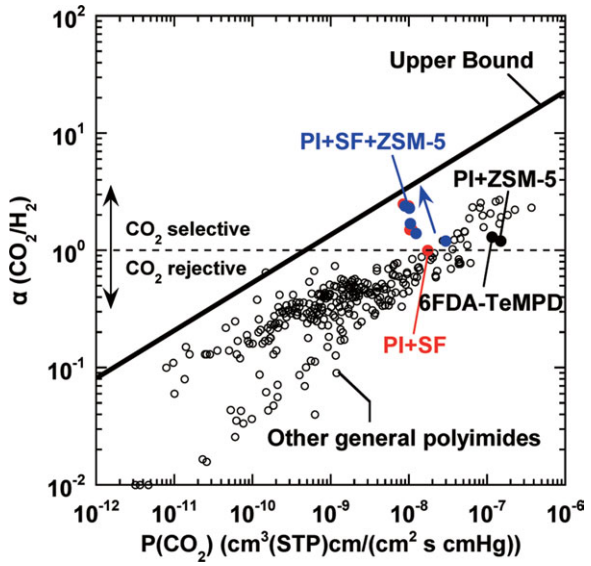

Figure 11. CO_2/H_2 separation performance of PI membranes at 35°C with a recent upper bound.[36,37] [Color figure can be viewed in the online issue, which is available at wileyonlinelibrary.com.]

SF contents. Thus, the SF content in the PI+ZSM-5+SF membrane reduced the level of interface defects and subsequently increased the CO_2 selectivity.

Figure 11 shows the CO_2/H_2 performance of each PI membrane at 35°C. The upper bound of CO_2/H_2 is cited from Refs. 36 and 37. The general aromatic PI membranes show lower CO_2/H_2 separation performance because of the generally higher permeability of H_2 when compared with those of the other gas molecules. Our data show that the CO_2/H_2 performance enhanced with the increase in the SF content. For example, the PI+ZSM-5+SF (33 wt%) membrane is located near the upper bound. Therefore, the use of liquid SF could be an effective approach to preventing the formation of interface defects and increasing the CO_2 selectivity, particularly for CO_2/H_2.

CONCLUSIONS

Novel, free-standing composite membranes consisting of 6FDA-TeMPD PI, 33 wt % liquid SF, and zeolite were prepared via the casting method to improve the interface defects between the PI and the zeolite. TG analysis shows that the PI+ZSM-5+SF membrane increased the decomposition temperature of PI, suggesting that the zeolite improved the thermal stability of the PI. The gas permeability of the PI+ZSM-5 membrane was higher than that of PI, whereas the gas selectivity was significantly reduced. These results can be attributed to the interface defects between the PI and the zeolite. Regardless of the SF content, the gas permeability of the PI+ZSM-5+SF membranes was higher than those of the PI+SF membranes due to interface defects. The defects causes the decrease in gas selectivity but can be reduced the level of defects through the introduction of SF. The gas selectivities for CO_2/H_2 and CO_2/N_2 of the PI+ZSM-5+SF and PI+SF membranes increased with the increase in the SF content. These results suggest that the addition of liquid SF and ZSM-5 zeolite in the PI+ZSM-5+SF membranes addressed the interface defects and increased the gas permeability and CO_2 selectivity. Furthermore, the selectivity for CO_2/H_2 of the PI+ZSM-5+SF membranes is located near the recent upper bound in this study.

ACKNOWLEDGMENTS

This research was partially supported by a Grant-in-aid for Scientific Research C (24560862) from the Ministry of Education, Culture, Sports, Science and Technology, Japan, the Japanese Society of the Promotion of Science, Research Project Grant B (3) from the Institute of Science and Technology, Meiji University, Japan, and Grant-in-Aid for the Japan Society for the Promotion of Science (JSPS) Fellows (2410856).

REFERENCES

1. Baker, R. W., Ed. In Membrane Technology and Applications; McGraw-Hill: New York, **2000**.
2. Freeman, B. D.; Yampolskii, Y., Ed. In Membrane Gas Separation; Wiley: Chichester, West Sussex, **2010**.
3. Bernardo, P.; Drioli, E.; Golemme, G. *Ind. Eng. Chem. Res.* **2009**, *48*, 4638.
4. Xiao, Y.; Low, B. T.; Hosseini, S. S.; Chung, T. S.; Paul, D. R. *Prog. Polym. Sci.* **2009**, *34*, 561.
5. Miyata, S.; Sato, S.; Nagai, K.; Nakagawa, T.; Kudo, K. *J. Appl. Polym. Sci.* **2008**, *107*, 3933.
6. Kanehashi, S.; Nakagawa, T.; Nagai, K.; Duthie, X.; Kentish, S.; Stevens, G. *J. Membr. Sci.* **2007**, *298*, 147.
7. Pechar, T. W.; Kim, S.; Vaughan, B.; Marand, E.; Tsapatsis, M.; Jeong, H. K.; Cornelius, C. J. *J. Membr. Sci.* **2006**, *277*, 195.
8. Pechar, T. W.; Tsapatsis, M.; Marand, E.; Davis, R. *Desalination* **2002**, *146*, 3.
9. Hibshman, C.; Cornelius, C. J.; Marand, E. *J. Membr. Sci.* **2003**, *211*, 25.
10. Yong, H. H.; Park, H. C.; Kang, Y. S.; Won, J.; Kim, W. N. *J. Membr. Sci.* **2001**, *188*, 151.
11. Hillock, A. M. W.; Miller, S. J.; Koros, W. J. *J. Membr. Sci.*, **2008**, *314*, 193.
12. Zornoza, B.; Carlos, T.; Coronas, J. *J. Membr. Sci.* **2011**, *368*, 100.
13. Cornelius, C. J.;Marand, E. *J. Membr. Sci.* **2002**, *202*, 97.
14. Cornelius, C. J.;Marand, E. *Polymer* **2002**, *43*, 2385.
15. Vu, D. Q.; Koros, W. J.; Miller, S. J. *J. Membr. Sci.* **2003**, *211*, 311.
16. Vu, D. Q.; Koros, W. J.; Miller, S. J. *J. Membr. Sci.* **2003**, *221*, 233.
17. Aroon, M. A.; Ismail, A. F.; Montazer-Rahmati, M. M.; Matsuura, T. *J. Membr. Sci.* **2010**, *364*, 309.
18. Chung, T.-S.; Jiang, L. Y.; Li, Y.; Kulprathipanja, S. *Prog. Polym. Sci.* **2007**, *32*, 483.
19. Aroon, M. A.; Ismail, A. F.; Montazer-Rahmati, M. M.; Matsuura, T. *Sep. Purif. Tech.* **2010**, *775*, 229.

20. Mahajan, R.;Koros, W. *J. Polym. Eng. Sci.* **2002**, *42*, 1420.
21. Sen, D.; KalIpcilar, H.; Yilmaz, L. *J. Membr. Sci.* **2007**, *303*, 194.
22. Murat, S.; Nurcan, B.; Levent, Y. *J. Membr. Sci.* **1994**, *91*, 77.
23. Duval, J. M.; Kemperman, A. J. B.; Folkers, B.; Mulder, M. H. V.; Desgrandchamps, G.; Smolders, C. A. *J. Appl. Polym. Sci.* **1994**, *54*, 409.
24. Moore, T. T.; Koros, W. J. *J. Mol. Struct.* **2005**, *739*, 87.
25. Li, Y.; Guan, H.-M.; Chung, T.-S.; Kulprathipanja, S. *J. Membr. Sci.* **2006**, *275*, 17.
26. Patel, R.; Park, J. T.; Hong, H. P.; Kim, J. H.; Min, B. R. *Polym. Adv. Technol.* **2011**, *22*, 768.
27. Li, J.; Nagai, K.; Nakagawa, T.; Wang, S. *J. Appl. Polym. Sci.* **1996**, *61*, 2467.
28. Li, J.; Tachihara, K.; Nagai, K.; Nakagawa, T.; Wang, S. *J. Appl. Polym. Sci.* **1996**, *60*, 1645.
29. Hao, J.; Tanaka, K.; Kita, H.; Okamoto, K.-I. *J. Polym. Sci. Part A: Polym. Chem.* **1998**, *36*, 485.
30. Popescu, V.; Oprea, C.; Birghila, S. *Rom. J. Phys.* **2006**, *51*, 293.
31. Olson, D. H.; Kokotailo, G. T.; Lawton, S. L.; Meier, W. M. *J. Phys. Chem.* **1981**, *85*, 2238.
32. Harrick, N. J., Ed. In Internal Reflection Spectroscopy; Interscience: New York, **1967**.
33. Sato, S.; Ose, T.; Miyata, S.; Kanehashi, S.; Ito, H.; Matsumoto, S.; Iwai, Y.; Matsumoto, H.; Nagai, K. *J. Appl. Polym. Sci.* **2011**, *121*, 2794.
34. Komatsuka, T.;Nagai, K. *Polym. J.* **2009**, *41*, 455.
35. Sawada, H.; Takahashi, Y.; Miyata, S.; Kanehashi, S.; Sato, S.; Nagai, K. *Trans. Mater. Res. Soc. Jpn.* **2010**, *35*, 241.
36. Jansen, J. C.; Friess, K.; Clarizia, G.; Schauer, J.; Izák, P. *Macromolecules* **2010**, *44*, 39.
37. Patel, N. P.; Hunt, M. A.; Lin-Gibson, S.; Bencherif, S.; Spontak, R. J. *J. Membr. Sci.* **2005**, *251*, 51.